

1 **Use of remote-sensing to quantify the distribution of**
2 **progradation/erosion along a forced-regressive modern coastline:**
3 **driving factors and impact on the stratigraphic record**

4 Valentin Zuchuat¹, Miquel Poyatos-Moré², Björn Nyberg^{3,4}, Rachel A. Nanson⁵, Stephen
5 Sagar⁵, Leo Lymburner⁵, Robbi Bishop-Taylor⁵

6 ¹Geological Institute, RWTH-Aachen University, Wüllnerstrasse 2, Aachen, 52062 Germany

7 ²Departament de Geologia, Universitat Autònoma de Barcelona, 08193 Cerdanyola del Vallès, Spain

8 ³Department of Earth Sciences, University of Bergen, Allégaten 41, 5007 Bergen, Norway

9 ⁴Bjerknes Centre for Climate Research, Allegaten 70, 5020, Bergen, Norway

10 ⁵National Earth and Marine Observations Branch, Geoscience Australia, Cnr Jerrabomberra Ave and Hindmarsh
11 Drive, Symonston ACT 2609, Australia

12

13 This manuscript on EarthArxiv has not been peer-reviewed yet, as two reviewers are handling
14 it after we submitted it to *The Sedimentary Record* on the 5th December 2022.

15

16 **ABSTRACT**

17 The long-term development of ancient and modern coastal distributary fluvial systems (DFSs)
18 during periods of relative sea-level highstand or fall usually drive net-progradation of
19 shorelines, though such deposits usually also record annual to millennial-scale deviations in
20 coastal trajectories. A new continental dataset (Digital Earth Australia Coastlines: DEA
21 Coastlines) provides an opportunity to examine such variations in coastal behaviour over
22 annual to decadal scales (1988-2019) and over vast spatial scales. This dataset is herein
23 applied to the 654 km coastline fronting Australia's largest amalgamated coastal distributary
24 fluvial systems, which is situated in the epicontinental seaway of the Gulf of Carpentaria.
25 Despite the overall forced regressive conditions, only 54% of this coastlines length net-
26 prograded, whereas 47% was eroded. Though temporal cyclicity in progradation and erosion
27 is evident along segments of this coast, these patterns could not be correlated with either the
28 Southern Oscillation Index ($R^2 = -0.20$) or rainfall ($R^2 = 0.24$). Instead, short-term coastline
29 dynamics appear to be the result of complex interactions between fluvial, wave, longshore
30 current, and tidal processes. The high-resolution DEA Coastlines dataset highlights the
31 diachronous, heterochronous, composite, and amalgamated nature of net-progradational
32 stratigraphic strata that can develop in shallow-marine environments where hinge-points
33 between progradating and retrograding coastal segments are dynamic features that migrate
34 with time. Understanding more granular temporal and spatial deviations in coastal trajectory
35 will help to improve models of such complex net-progradational coastal systems.

36 **Key words:** Forced regression, DEA Coastlines, Gulf of Carpentaria, progradation, erosion,
37 bounding surface

38 INTRODUCTION

39 Coastal systems are shaped by temporally-variable cycles of erosion and deposition that
40 contribute to the incompleteness and heterogeneity in the stratigraphic record. Such erosion-
41 deposition cycles are recorded in the landscape by the development of beach ridges and
42 cheniers (Semeniuk, 1995; Tamura, 2012). Annual to multi-decadal events and cycles (e.g.
43 the El Niño–Southern Oscillation (ENSO), the Pacific Decadal Oscillation (PDO), the Atlantic
44 Multi-decadal Oscillation (AMO), Dansgaard-Oeschger (DO), or DO-like events (see Boulila et
45 al., 2022) likely contribute to such gaps, owing to: (i) the complex nature of these cycles (both
46 for cause(s) and consequences); (ii) the along-strike variability of coastal dynamics; (iii) the
47 highly-variable preservation potential of sediments; and (iv) the increasing loss of time
48 resolution and calibration with age. Detailed studies of modern analogue coastal sedimentary
49 systems that examine these processes can be used to inform longer-term analyses for a range
50 of end-users (e.g. basin analyses, policy makers).

51 Coastline trajectories reflect the ratio between the rates of accommodation creation (A) and
52 sediment supply (S) (Helland-Hansen and Martinsen, 1996): progradation occurs when $A < S$,
53 with $A > 0$ (i.e. during a normal regression) or when $A < 0$ (i.e. during a period of relative sea-
54 level fall: forced regression). However, the study of modern marginal-marine systems has
55 demonstrated that the spatial and temporal distribution of sediment supplied and the
56 combination of oceanic processes play important roles in the along-strike and dip variability in
57 coastal dynamics (Nanson et al., 2013; Nyberg and Howell, 2016; Lane et al., 2017). Waves
58 and tides can remobilise and redistribute sediments along- and off-shore, and these changes
59 vary by temporal and spatial fluctuations in the frequency and intensity of wave, tide and fluvial
60 processes (see discussion in Overeem et al., 2022). Consequently, coastline trajectories can
61 vary markedly along individual isochrones, which can be simultaneously prograding and
62 retrograding either side of hinges or pivot points (Madof et al., 2016; Nanson et al., 2022).

63 We utilise a multi-decadal remote-sensing dataset (Digital Earth Australia's Coastlines (DEA
64 Coastlines; Bishop et al., 2021) to investigate the complexity of annual to decadal coastal
65 dynamics fronting Australia's largest, amalgamated, Holocene, forced-regressive, fan-delta
66 deposits that have accumulated on the eastern shore of the Gulf of Carpentaria (GoC; Fig. 1).
67 High-frequency cyclic erosion and depositional styles and Holocene rates of progradation have
68 been well-documented for these systems (Rhodes, 1982; Jones et al., 1993, 2003; Nanson et
69 al., 2013; Massey et al., 2014; Lane et al., 2017; Porritt et al., 2020). The relatively limited
70 anthropogenic modification of these systems over the last 200 years (Nanson et al., 2013)
71 provides a natural laboratory to investigate the roles of various autogenic and allogenic controls
72 on coastal change, and to frame considerations of preservation potential in the stratigraphic
73 record.

74

75 **GEOLOGICAL SETTING**

76 The Gulf of Carpentaria (GoC) is an epicontinental seaway in Northern Australia, which
77 connected to the Arafura and Coral Seas to the north and is characterized by a low gradient
78 and bathymetry (< 70m; Torgersen et al., 1983). Drainage catchments initiate in the Great
79 Dividing Range to the east and have created four large and amalgamated Distributive Fluvial
80 Systems (DFSs; Gilbert, Staaten, Mitchell, and Coleman). The deltas of these DFSs are mixed-
81 influence (wave, tide, and fluvial), with peak fluvial discharge during the monsoonal season
82 (December-March; Australian Bureau of Meteorology (BoM)). Sea-level fall, low-gradient
83 bathymetry, and increased sedimentation during the past 4 ka has led to between ca. 0.84
84 km/kyr to ca. 3 km/kyr of forced-regressive delta progradation, which varies both in time and
85 space (Nanson et al., 2013; Lane et al., 2017; Porritt et al., 2020).

86 Tides in the GoC are diurnal (Neil et al., 2021) and mesotidal, with maximum range of 4 m near
87 Karumba (Hopey and Smithers, 2010; Figure 1a). Significant wave height (*sensu* Munk and
88 Arthur, 1951) over the past 30 years extracted from nine control points along the studied
89 coastline (Wavewatch III®) reaches ca. 30 cm, although storm wave height are expected to be
90 much greater (3.5 m peak height in the monsoon; Nanson et al., 2013). Sediment flux data is
91 sparse between rivers. The Gilbert River (Fig. 1) has been estimated to supply ca 1 Mm³/yr
92 since the start of the Holocene (Porritt et al., 2020), and models of the Mitchell River predicted
93 2.9 Mt/yr of silt and clay reaching the GoC (Rustomji et al., 2010).

94

95 **METHODS**

96 The DEA Coastlines dataset contains yearly point series linked to lines that show the dominant
97 median annual position of the coastline at 0 m annual mean sea level for each year between
98 1988-2019 (Bishop-Taylor et al., 2021). Datapoints were derived every 30 m along the whole
99 of Australia's coastline from the Digital Earth Australia archive of Landsat satellite images (Dhu
100 et al., 2017). These were constrained by pixel-based tidal modelling to avoid artefacts
101 associated with varied tidal stages at the time satellite imagery was acquired, in order to
102 generate a smooth coastline every year for the whole of Australia (Bishop-Taylor et al., 2021).
103 The final dataset was then successfully validated by comparing it to independently measured
104 coastline positions around Australia (Bishop-Taylor et al., 2021). It also contains average rates
105 of progradation for every data point along the coastline (positive rates of progradation = actual
106 progradation; negative rates of progradation = erosion).

107 Yearly data along the targeted segment between Karumba and Aurukun were directly exported
108 from the main DEA Coastlines dataset (coordinates: 140.82801°E/-17.46528°S to
109 141.69620°E/-13.26780°S; detail python script in Appendix A). The overall coastal
110 progradation between 1988-2019 was plotted from this dataset after each yearly sub-dataset
111 was averaged along a 100 m rolling window (Fig. 1A). The average rates of progradation

112 between 1988-2019 (Fig. 1B) were plotted using a modified ShowYourStripes script originally
113 developed by Maximilian Nöthe (modified script in Appendix B). The difference in position
114 between each year was calculated for each data point from the 100-m-averaged sub-dataset
115 (Fig. 1C), and colour-coded in red if the coastline retreated between two subsequent years, or
116 in blue if the coastline prograded (script used to generate plot available in Appendix C).

117 Wave-energy data and direction of coastal progradation were collected using the from
118 Wavewatch III®, a hindcast average wave directions for the past 30 years (NOAA, 2022).
119 Precipitations and Southern Oscillation Index (SOI) data were downloaded from the Australian
120 Bureau of Meteorology (BoM, 2022). The total precipitation in each river catchment along the
121 GoC was calculated based on the delineations of Nyberg et al. (2018).

122

123 **RESULTS**

124 **Coastal behaviour (progradation vs erosion)**

125 Despite the overall forced regressive conditions of the GoC within the last 6000 years (Nanson
126 et al., 2013; Lane et al., 2017; Sloss et al., 2018; Porritt et al., 2020), the shorter-term behaviour
127 of the studied coastal segment is heavily heterogeneous, both in terms of spatial distribution
128 and magnitude of change. Only 54.23 % of the coastline length experienced a net progradation
129 between 1988-2019, whereas 47.77 % was eroded. A majority of the total coastline movement
130 over the 32 years of observations was between -100 and +100 m (87%); exceptional
131 progradation reached a maximum of 372 m, whereas maximum observed erosion was 761 m
132 (Fig. 1A). The town of Pormpuraaw north of the Mitchell delta separates the progradation-
133 erosion results in two domains: i) the southern domain from Karumba to Pormpuraaw, and ii)
134 the northern domain, from Pormpuraaw to Aukurum (Fig. 1A). The southern domain is
135 characterised by greater progradation-erosion amplitudes (average progradation of 49.67 m
136 and average erosion of 54.48 m) than the northern domain between 1988-2019, where the
137 amplitude between progradation and erosion values are smaller (average progradation 13.85
138 m of and average erosion of 26.29 m). Additionally, coastlines near active river mouths in the
139 southern domain have been very mobile between 1988-2019. For example, the coastline on
140 the southern side of the Mitchell River mouth has moved over a distance of ca. 1 km between
141 1988-2019. This high degree of mobility rapidly decreases away from the river mouth towards
142 beaches and cheniers. About 46 % of the studied coastline experienced average rates of
143 progradation between -2 and 2 m/yr (Fig. 1B), extraordinarily reaching maximum rates of -60
144 and 34 m/yr. When averaged for the entire studied coastal segment between 1988-2019, 4.29
145 m of the coastal sediments were eroded between 1988-2019. This means that the average
146 rate of progradation for the entire studied coastline is -0.14 m/yr. The results do not provide,
147 however, a volumetric indication of how much sediment was eroded or deposited between
148 1988-2019. Figure 1C displays the yearly coastal erosional or progradational behaviour along

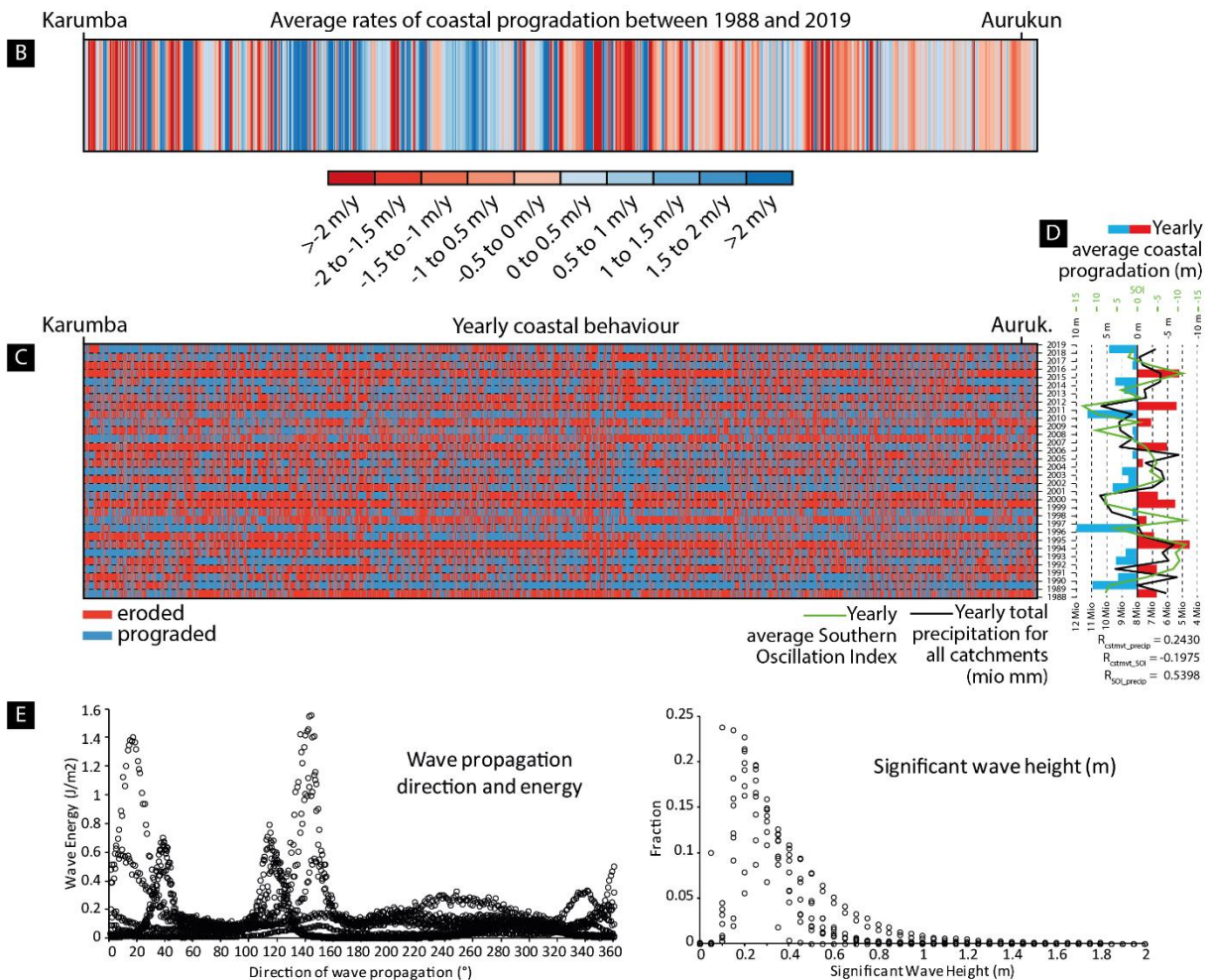
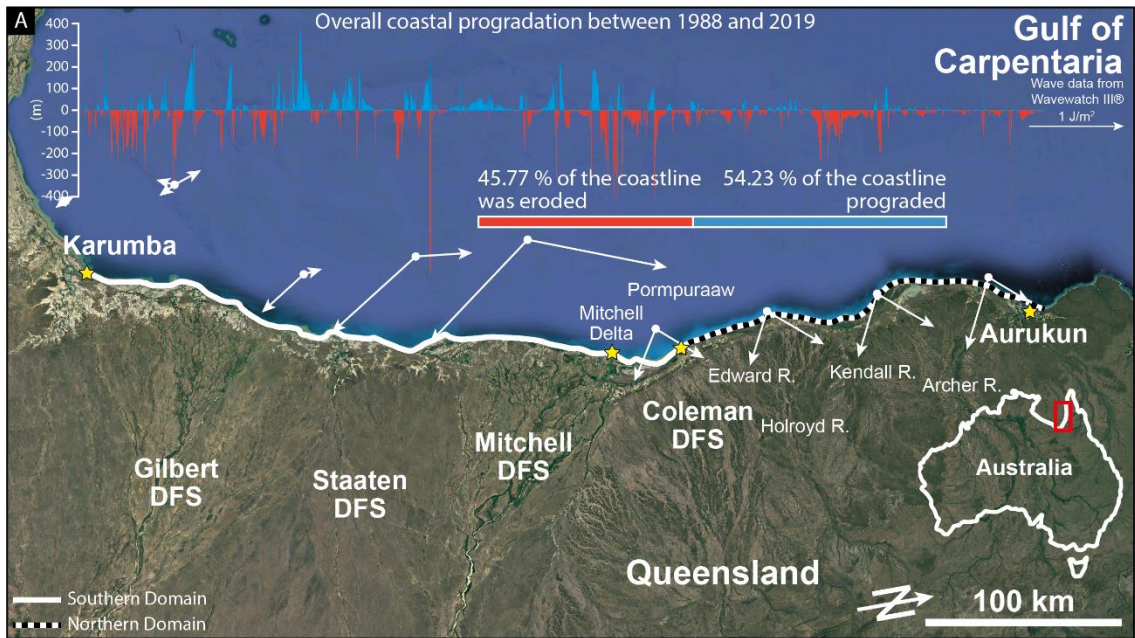
149 the studied section of the GoC, which can be regarded as a Wheeler diagram (Wheeler, 1958;
150 1964). This yearly coastal behaviour diagram, as well as the values of yearly coastal behaviour
151 averaged for the whole studied coastline (Fig. 1D) display a vague four to six years cyclical
152 alternation of periods dominated by coastal progradation versus periods dominated by coastal
153 erosion.

154 **Coastal progradation controls**

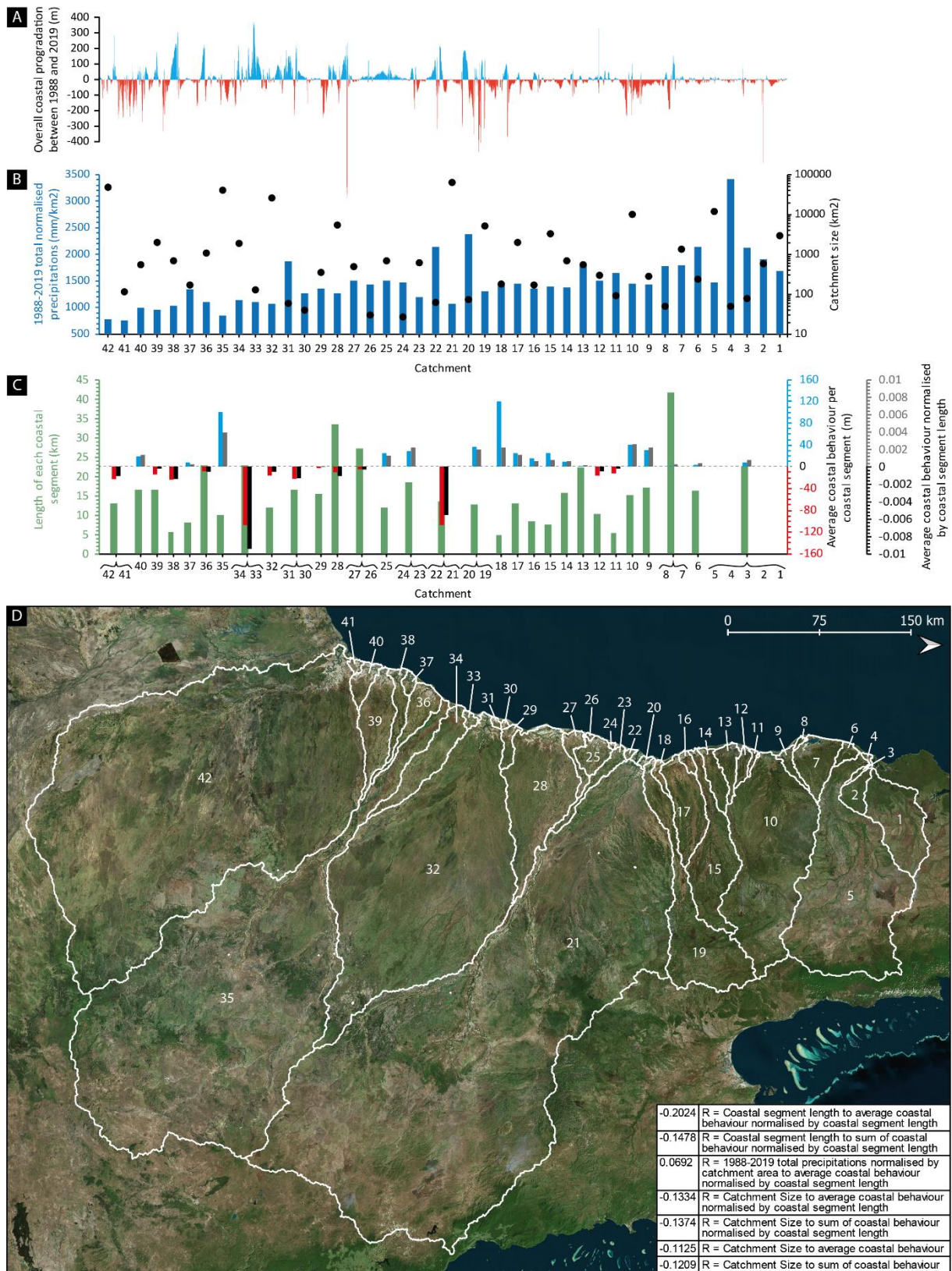
155 Total precipitations over all the catchments feeding rivers that reach the studied coastline also
156 show oscillating multi-year phases of high and low precipitations. Compared to the yearly-
157 averaged Southern Oscillation Index (SOI), precipitation is characterised by a R^2 value of 0.54,
158 in line with reported trends for Australia (Wu and Leonard, 2019). It seems, however, that the
159 cyclical pattern observed in the average coastal behaviour is poorly correlated to both the total
160 precipitations and the SOI, with R^2 values of 0.24 and -0.20 respectively (Fig. 1D).

161 Wave direction data show that most of the studied coastline is impacted by two sets of waves
162 propagating towards the NNE and SE/SSE (Fig. 1A, 1E; Supplementary Material A), reaching
163 a maximum energy level of 1.557 J/m^2 , while 75 % of the significant wave height are comprised
164 between 0.2 and 0.45 m at nine of the offshore data points. Between 1988-2019, 34 major
165 storms and tropical cyclones have affected the area, including the tropical cyclones Barry and
166 Ethel (1996), Abigail (2001), Grant (2011), Oswald (2013) and Nora (2018) (BoM; complete
167 list in Appendix D). Despite the scarcity of available data, some of these events were
168 associated with heavy rainfall, storm surges, high tides and waves (note: the nearest tide and
169 wave gauges is near Weipa, north of the studied coastal segment). For instance, Ethel
170 generated a storm surge of 1.18 m, with a significant wave height and a peak wave height of
171 3.76 m and 6.69 m respectively, while Nora generated a 1.2 m storm surge (BoM, 2022). The
172 storm surge that accompanied Barry destroyed a fishermen' camp, built 4 m above the high-
173 water mark, between the mouths of the Gilbert and the Staaten rivers, flooding up to 7 km
174 inland (BoM, 2022).

175 Precipitation, however, is not distributed equally across the hinterland of the studied coastline
176 (Fig. 2B), with more precipitation per surface unit in the northern than in the southern domain.
177 R^2 Statistical test results (Fig. 2D) show that both the average and the sum of coastal behaviour
178 per coastal segment associated with each catchment or group of catchments (normalised or
179 not) are independent of: (1) the size of each catchment ($R^2_{av} = 0.11$; $R^2_{sum} = 0.12$; $R^2_{av_norm} =$
180 0.13 ; $R^2_{sum_norm} = 0.14$); (2) the total amount of precipitations of each catchment normalised by
181 the size of each catchment ($R^2 = 0.07$); and (3) the length of the coastal segment associated
182 with each catchment or group of catchments ($R^2_{av_norm} = 0.20$; $R^2_{sum_norm} = 0.15$; Fig. 2B-D).



183
 184 Fig. 1 – (A) Spatial distribution of coastline progradation (in m) along the Queensland margin of the Gulf of Carpentaria where
 185 Gilbert, Staaten, Mitchell, and Coleman DFSs reach the sea. Continuous white line along the coast: Southern Domain; black-
 186 white dashed line along the coast: Northern Domain. White arrows indicate wave direction and their length is scaled to 1 J/m²
 187 (satellite imagery ©Google Earth). (B) average rates of coastline progradation between 1988-2019 (m/y). (C) Yearly coastal
 188 behaviour plots. (D) Yearly total precipitations for all catchments (Mio mm) plotted against the yearly average coastal
 189 behaviour (m), and the yearly average Southern Oscillation Index (SOI), with Pearson test results comparing the three
 190 parameters (precipitation and SOI data from BoM). (E) Wave direction of propagation, energy, and significant wave height
 191 (data extracted from Wavewatch III® using the Global Wave and Tide Data app developed by Jaap Nienhuis; see Fig. 1A for
 192 location of datapoints).



194
 195 Fig. 2 – Plot series comparing (A) the coastline progradation (in m) along the studied coastline to (B) the total 1988-2019
 196 precipitations of each catchment normalised by the surface of each catchment (blue bars). Black dots = actual size of each
 197 catchment. (C) Length of coastal segment associated with each catchment or group of catchments (green bars), average
 198 coastal behaviour per coastal segment of each catchment or group of catchments (red-blue bars), and average coastal
 199 coastal behaviour per coastal segment of each catchment or group of catchments normalised by the length of each coastal segment
 200 (light red-blue bars). (D) Outline of each river catchment, with Pearson test results comparing the different parameters (satellite
 201 imagery Bing based on TomTom, Earthstar Geographics SIO imagery (2022)).

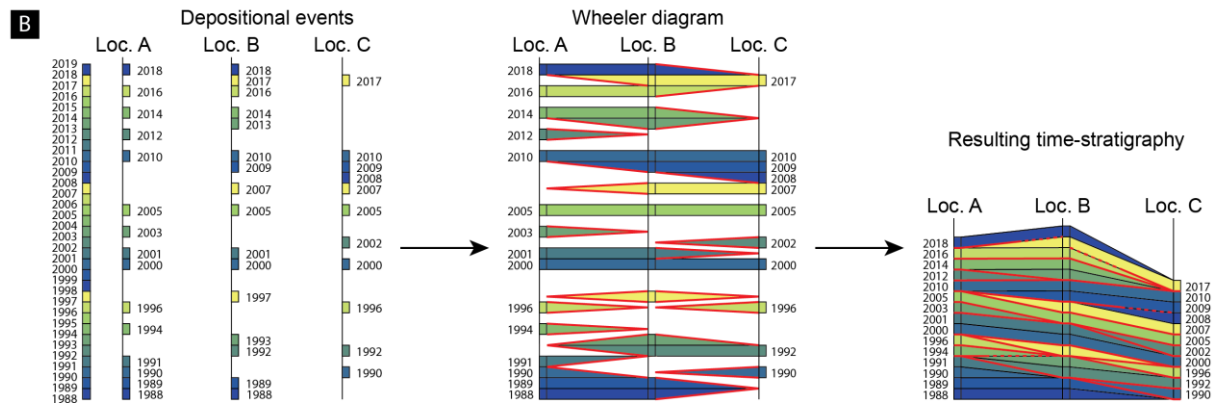
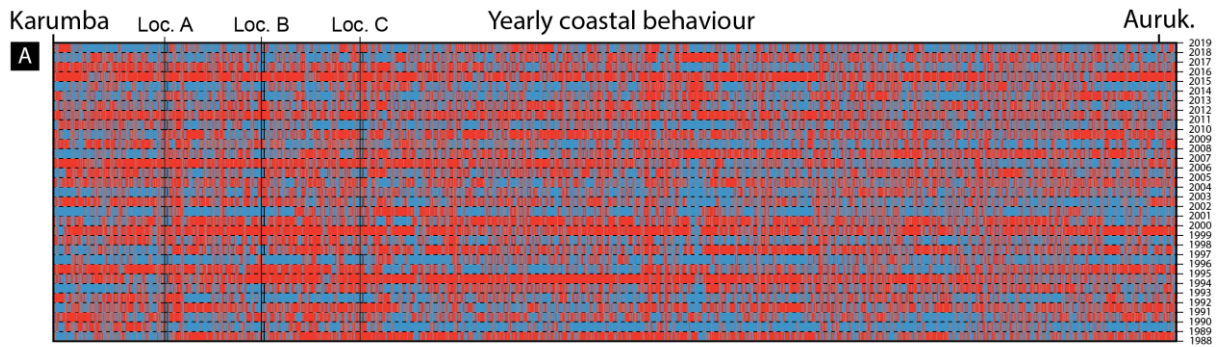
202

203 **DRIVING FACTORS AND PRESERVATION OF THE SIGNAL** 204 **IN THE ROCK RECORD**

205 DFSs are the loci of most of the sedimentation on land (Weissmann et al., 2010), and are very
206 often associated with a long-term prograding trend as the system grows from high sediment
207 input (e.g. Fisher et al., 2007; Davidson et al., 2013). This long-term prograding trend has been
208 recognised along the GoC (Nanson et al., 2013; Lane et al., 2017; Sloss et al., 2018; Porritt et
209 al., 2020). Our results, however, highlight that the short-term trend between 1988-2019 along
210 the studied coastline is not following the overall regressive trend, as nearly half the studied
211 coastline experienced erosion/transgression during a certain period of time. Nevertheless and
212 although most of the sediment is being supplied by different rivers reaching the GoC, the
213 behaviour of the total studied coastline does not correlate to the precipitation-proxied river
214 discharge to the shoreline. Rather than sediment supply alone, the dynamics of the coastline
215 between 1988-2019 seem to have been more dependent on the sum of fluvial, wave action,
216 longshore currents, and tidal processes along the studied system, but given a lack of detailed
217 historical wave, longshore current, and tidal data in the Gulf of Carpentaria, these factors could
218 not be studied in further detail. Furthermore, the i) nature of the substrate, as well as the spatial
219 distribution of cohesive clays (and other cohesive biogenic substances) along the coastline
220 (e.g. Lichtman, et al., 2018; Wu et al., 2022), ii) the change in gradient through time and space
221 associated with varying rates of relative sea-level change (Rodriguez et al., 2001; Ruggiero et
222 al., 2016), and iii) the type, rates of change, and degree of vegetation near the shoreline (e.g.
223 Thampanya et al., 2006; Konlechner et al., 2019) could certainly enhance or dampen the
224 overall mobility of the coastline (how much the coastline migrates) and the rates at which the
225 coastline moves (how fast the coastline migrates). Nevertheless, DFSs are affected by
226 continuous lateral channel migration or frequent avulsions at a kyr timescale (Porritt et al.,
227 2020; Colombera and Mountney, 2022) depending on grain size and sediment load (Cazanacli
228 et al., 2022), none of which occurred within the time frame covered by the DEA Coastline
229 dataset. Such avulsions would influence the spatial distribution of wave, tidal, and fluvial
230 processes along the coastline, as well as diverting the sediment supply. Thus, even though
231 shallow-marine processes actively redistributed the sediments along the studied coastline and
232 were the driving factors responsible its short-term dynamics, the influence of fluvial processes
233 might still be substantial, but more inferred or deferred rather than direct. As a result, the
234 quantification of each of the role/influence is blurred by the amalgamation of different
235 timescales, resulting in a potential over- or under-interpretation of the sedimentary processes
236 that acted at the time of deposition.

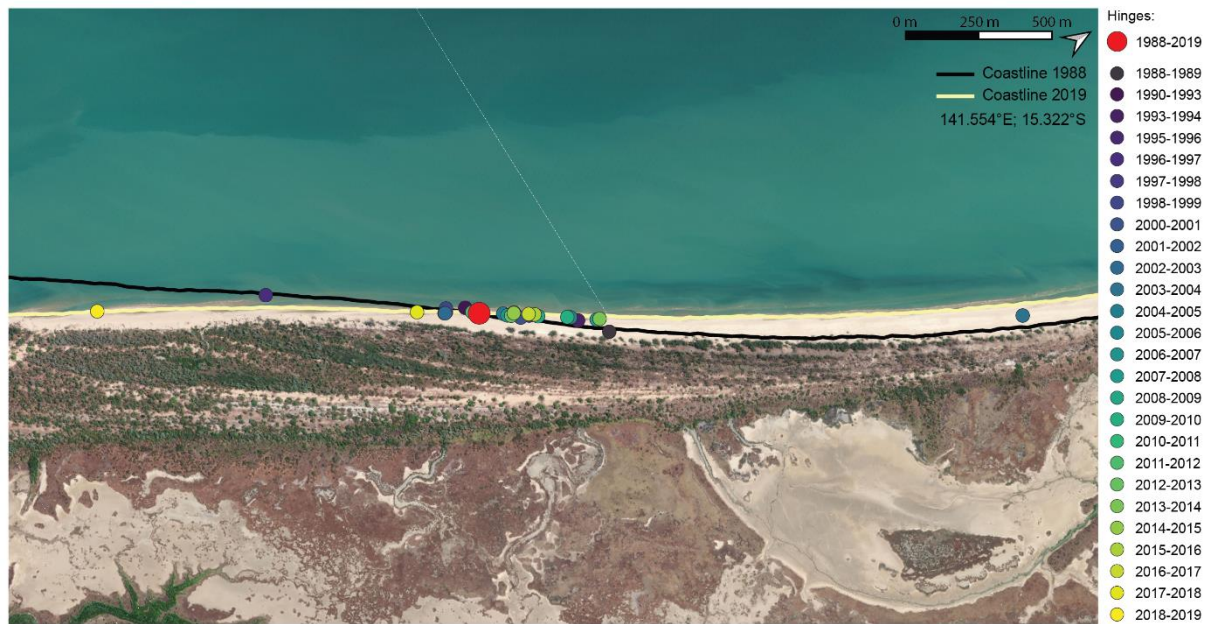
237 Results have shown how dynamic a segment of the coastline of GoC has been between 1988-
238 2019, regarding both spatial and temporal dimensions. Despite the lack of volumetric
239 quantification of the erosion and progradation phases limits our ability to answer precisely “how
240 much of this signal is preserved in the rock record”, these results highlight that the highly-

241 variable and unpredictable short-term dynamics of these systems, and allow the following
242 question to be raised: is there a minimum spatial and temporal scale below which
243 progradational or retrogradational trends cannot be differentiated? In other words, at what
244 moment does time sufficiently amalgamate through space for a general, basin-wide trend to
245 emerge, or when does the overall sum of local progradation (or erosion) reaches the threshold
246 that allows general trends to be identified? This dataset covers the last 30 years, which in
247 geological terms is virtually instantaneous, and the coastline behaviour suggests it cannot be
248 characterised as undergoing a forced regression at this time scale. Indeed, the average rate
249 of coastal progradation between 1988-2019 is -0.14 m/yr. Although being spatially extremely
250 variable, this average rate of coastal progradation suggest a short-term average reversal or of
251 the coastal behaviour when compared to the longer-term Holocene progradational rates
252 ranging between 0.84 m/yr to ca. 3.0 m/yr, and accelerating to 3.8 m/yr in the last 400 years
253 (Nanson et al., 2013; Porritt et al., 2020). The exact explanation as of why this 1988-2019
254 average rate of coastal progradation is so different from the longer-term Holocene
255 progradational rates goes beyond the scope of this manuscript. Also, the resulting time-
256 stratigraphy is completely different from one location to another along the studied coastline
257 segment (Fig. 3). As a consequence of this, stratigraphic surfaces bounding coastal strata
258 developed in different years are heavily diachronous (through time) and heterochronous (at
259 different time), composite, and amalgamated (i.e. regressive surfaces, flooding surfaces; Fig.
260 3). This is not a new concept in stratigraphy (e.g. Kyrkjebø et al., 2004; Holbrook and
261 Bhattacharya, 2012; Miall, 2016; Gani, 2017; Zuchuat et al., 2019). In addition to diachronous
262 and heterochronous nature of these surfaces, our results show that hinges between areas of
263 progradation and retrogradation are dynamic features that migrate spatially depending on the
264 temporal scale considered (Fig. 4). The consequence of the spatial migration of these hinges
265 is that, on each side of a “time-averaged” hinge (i.e. the type of hinge usually available in the
266 sedimentary record), the preserved stratigraphy can display characteristics of short-term
267 transgression and regression on each side of the hinge, even though the longer-term trend of
268 one side of the hinge is prograding and the other one is transgressing. Because sequence
269 stratigraphic units are defined “by stratal stacking patterns and specific bounding surfaces, and
270 not by their inferred controls, age, time span, or physical scales” (Catuneanu, 2019, p. 135),
271 these migrating hinges will further encumber the often-oversimplified lateral correlation of
272 these stratigraphic surfaces. Despite the increased complexity, implementing this concept of
273 migrating hinges can help refining the interpretation of the architecture of the preserved strata,
274 as well as the distribution of heterogeneities in the stratigraphy, and increase therefore
275 increase the robustness of basin models.



276
277 Fig. 3 – (A) Yearly coastal behaviour plot and (B) pseudo-logs illustrating the various depositional events occurring at each of
278 the locations, as well as the resulting time stratigraphy and the degree of amalgamation of stratigraphic surfaces.

279



280
281 Fig. 4 – Detailed photograph of a segment of the studied coastline indicating the position of the hinges between zones of
282 progradation and zones of erosion through time (satellite imagery Bing based on TomTom, Earthstar Geographics SIO imagery
283 (2022)).

284

285 CONCLUSIONS

286 The yearly movements of a 654.63 km segment of the Queensland coastline along the Gulf of
287 Carpentaria between Karumba and Aurukun were calculated using the Digital Earth Australia
288 Coastlines data between 1988-2019. Results show that:

- 289
- 290
- 291
- 292
- 293
- 294
- 295
- 296
- 297
- 298
- 299
- 300
- 301
- 302
- 303
- 304
- 305
- 306
- 307
- 308
- 309
- The mean average rate of coastline progradation for the study area is -0.14 m/yr using the DEA Coastlines dataset. This average rate encompasses considerable spatial and temporal variability.
 - Only 54.23 % of the coastline length net-prograded between 1988-2019, whereas 47.77 % was net-eroded, with most of coastline prograding or retreating by 100 m, at progradation rates mostly comprised between -2 and 2 m/yr.
 - Multi-year overall progradation-erosion cycles correlate poorly to both Southern Oscillation Index and the total precipitations recorded over the study area (used a proxy for sediment supply). The dynamics of the studied coastline between 1988-2019 seem to have been therefore more dependent on the sum of fluvial, wave action, longshore currents, and tidal processes rather than sediment supply alone.
 - Hinges between areas of progradation and retrogradation are dynamic features that migrate depending on the temporal scale considered. The intricate nature of stratigraphic surfaces developing on each side of hinges in such dynamic shallow-marine environments makes their lateral correlation difficult. The documented short-term coastal behaviour will encumber longer-term basin reconstructions and sequence stratigraphic analysis, because of the amalgamation of various timescales occurring along the system. Nevertheless, a better understanding of the temporal and spatial complexity and the dynamics of net-progradational coastal systems and the implementation of this complexity in geomodels will help increase their robustness.

310 **ACKNOWLEDGMENTS**

311 The authors would like to acknowledge the XXXX reviewers for their fruitful comments that
312 have improved the quality of this manuscript.

313

314 **DATA AVAILABILITY**

315 All the Digital Earth Australia Coastlines data are publicly and freely available at:
316 <https://cmi.ga.gov.au/data-products/dea/581/dea-coastlines#access>. The python codes used
317 for Appendix A: total progradation between 1988-2019 (Fig. 1A); Appendix B: progradation
318 rates (Fig. 1B); and Appendix C: Wheeler diagram (Fig. 1D) are all available on GitHub:
319 <https://github.com/Stratival/QueenslandCoastlineGoC>. The table of tropical cyclones that
320 affected the area between 1988-2019 (Appendix D) are attached to the online version of this
321 article. Precipitation and tropical cyclone data are both downloaded from on the BoM website:
322 [http://www.bom.gov.au/jsp/ncc/climate_averages/decadal-](http://www.bom.gov.au/jsp/ncc/climate_averages/decadal-rainfall/index.jsp?mctype=6&period=7605&product=totals#maps)
323 [rainfall/index.jsp?mctype=6&period=7605&product=totals#maps](http://www.bom.gov.au/jsp/ncc/climate_averages/decadal-rainfall/index.jsp?mctype=6&period=7605&product=totals#maps) and
324 <http://www.bom.gov.au/cyclone/tropical-cyclone-knowledge-centre/history/past-tropical->

325 [cyclones/](https://polar.ncep.noaa.gov/waves/hindcasts/). Wavewatch III® data and information available at:
326 <https://polar.ncep.noaa.gov/waves/hindcasts/>

327

328 **CONFLICT OF INTEREST**

329 The authors declare no conflict of interests.

330

331 **REFERENCES**

332 Bishop-Taylor, R., Nanson, R., Sagar, S., & Lymburner, L. (2021). Mapping Australia's
333 dynamic coastline at mean sea level using three decades of Landsat imagery. *Remote Sensing*
334 *of Environment*, 267, 112734.

335 Boulila, S., Galbrun, B., Gardin, S., & Pellenard, P. (2022). A Jurassic record encodes an
336 analogous Dansgaard–Oeschger climate periodicity. *Scientific Reports*, 12(1), 1-16.

337 Catuneanu, O. (2019). Scale in sequence stratigraphy. *Marine and Petroleum Geology*, 106,
338 128-159.

339 Cazanacli, D., Paola, C., & Singh, A. (2022). Sediment Load and Grain Size Controls on
340 Channel Migration Patterns in Experimental Deltas. *Journal of Geophysical Research: Earth*
341 *Surface*, e2021JF006402.

342 Colombera, L., & Mountney, N. P. (2022). Scale dependency in quantifications of the avulsion
343 frequency of coastal rivers. *Earth-Science Reviews*, 104043.

344 Davidson, S. K., Hartley, A. J., Weissmann, G. S., Nichols, G. J., & Scuderi, L. A. (2013).
345 Geomorphic elements on modern distributive fluvial systems. *Geomorphology*, 180, 82-95.

346 Dhu, T., Dunn, B., Lewis, B., Lymburner, L., Mueller, N., Telfer, E., Lewis, A., McIntyre, A.,
347 Minchin, S. and Phillips, C., 2017. Digital earth Australia—unlocking new value from earth
348 observation data. *Big Earth Data*, 1(1-2), pp.64-74.

349 Fisher, J. A., Nichols, G. J., & Waltham, D. A. (2007). Unconfined flow deposits in distal sectors
350 of fluvial distributary systems: examples from the Miocene Luna and Huesca Systems,
351 northern Spain. *Sedimentary Geology*, 195(1-2), 55-73.

352 Gani, M. R. (2017). Mismatch between time surface and stratal surface in stratigraphy. *Journal*
353 *of Sedimentary Research*, 87(11), 1226-1234.

354 Hartley, A. J., Weissmann, G. S., Nichols, G. J., & Warwick, G. L. (2010). Large distributive
355 fluvial systems: characteristics, distribution, and controls on development. *Journal of*
356 *Sedimentary Research*, 80(2), 167-183.

357 Helland-Hansen, W., & Martinsen, O. J. (1996). Shoreline trajectories and sequences;
358 description of variable depositional-dip scenarios. *Journal of Sedimentary Research*, 66(4),
359 670-688.

360 Holbrook, J. M., & Bhattacharya, J. P. (2012). Reappraisal of the sequence boundary in time
361 and space: case and considerations for an SU (subaerial unconformity) that is not a sediment
362 bypass surface, a time barrier, or an unconformity. *Earth-Science Reviews*, 113(3-4), 271-302.

363 Hopley, D., & Smithers, S. (2010). Queensland. In Bird, C.F. (ed.), *Encyclopedia of the World's*
364 *Coastal Landforms*. Springer Science+Business Media, Dodrecht, 1255-1266.

365 Jones, B.G., Martin, G.R. & Senapati, N. (1993). Riverine—tidal interactions in the monsoonal
366 Gilbert River fandelta, northern Australia. *Sedimentary Geology*, 83(3-4), 319-337.

367 Jones, B.G., Woodroffe, C.D., & Martin, G.R. (2003). Deltas in the Gulf of Carpentaria,
368 Australia: forms, processes and products. In Sidi, F.H., Nummedal, D., Imbert, P. Darman, H.
369 & Posamentier, H.W. (eds), *Tropical Deltas of Southeast Asia- Sedimentology, Stratigraphy*
370 *and Petroleum Geology*. SEPM (Society for Sedimentary Geology) Special Publication, 76,
371 21-43.

372 Kyrkjebø, R., Gabrielsen, R. H., & Faleide, J. I. (2004). Unconformities related to the Jurassic–
373 Cretaceous synrift–post-rift transition of the northern North Sea. *Journal of the Geological*
374 *Society*, 161(1), 1-17.

375 Konlechner, T. M., Kennedy, D. M., Cousens, R. D., & Woods, J. L. (2019). Patterns of early-
376 colonising species on eroding to prograding coasts; implications for foredune plant
377 communities on retreating coastlines. *Geomorphology*, 327, 404-416.

378 Lane, T. I., Nanson, R. A., Vakarelov, B. K., Ainsworth, R. B., & Dashtgard, S. E. (2017).
379 Evolution and architectural styles of a forced-regressive Holocene delta and megafan, Mitchell
380 River, Gulf of Carpentaria, Australia. In Hampson, G. J., Reynolds, A. D., Kostic, B., & Wells,
381 M. R. (eds), *Sedimentology of Paralic Reservoirs: Recent Advances*. Geological Society,
382 London, Special Publications, 444(1), 305-334.

383 Lichtman, I. D., Baas, J. H., Amoudry, L. O., Thorne, P. D., Malarkey, J., Hope, J. A., ... & Ye,
384 L. (2018). Bedform migration in a mixed sand and cohesive clay intertidal environment and
385 implications for bed material transport predictions. *Geomorphology*, 315, 17-32.

386 Madof, A. S., Harris, A. D., & Connell, S. D. (2016). Nearshore along-strike variability: Is the
387 concept of the systems tract unhinged?. *Geology*, 44(4), 315-318.

388 Massey, T.A., Fernie, A.J., Ainsworth, R.B., Nanson, R.A. and Vakarelov, B.K. (2014). Detailed
389 mapping, three-dimensional modelling and upscaling of a mixed-influence delta system,
390 Mitchell River delta, Gulf of Carpentaria, Australia. In Martinius, A.W., Howell, J.A., & Good,

391 T.R. (eds), *Sediment-Body Geometry and Heterogeneity: Analogue Studies for Modelling the*
392 *Subsurface*. Geological Society, London, Special Publications, 387(1), 135-151.

393 Miall, A. D. (2016). The valuation of unconformities. *Earth-Science Reviews*, 163, 22-71.

394 Munk, W. H., & Arthur, R. S. (1951). Forecasting ocean waves. In Malone, T.F. (ed.),
395 *Compendium of Meteorology*. American Meteorological Society, Boston, MA, 1082-1089.

396 Nanson, R. A., Vakarelov, B. K., Ainsworth, R. B., Williams, F. M., & Price, D. M. (2013).
397 Evolution of a Holocene, mixed-process, forced regressive shoreline: the Mitchell River delta,
398 Queensland, Australia. *Marine Geology*, 339, 22-43.

399 Nanson, R., Bishop-Taylor, R., Sagar, S., & Lymburner, L. (2022). Geomorphic insights into
400 Australia's coastal change using a national dataset derived from the multi-decadal Landsat
401 archive. *Estuarine, Coastal and Shelf Science*, 265, 107712.

402 Neill, S. P., Hemer, M., Robins, P. E., Griffiths, A., Furnish, A., & Angeloudis, A. (2021). Tidal
403 range resource of Australia. *Renewable Energy*, 170, 683-692.

404 Nyberg, B. (2019). Source to Sink Database. <https://doi.org/10.7910/DVN/ETH8VN>

405 Nyberg, B., & Howell, J. A. (2016). Global distribution of modern shallow marine shorelines.
406 Implications for exploration and reservoir analogue studies. *Marine and Petroleum Geology*,
407 71, 83-104.

408 Nyberg, B., Gawthorpe, R. L., & Helland-Hansen, W. (2018). The distribution of rivers to
409 terrestrial sinks: Implications for sediment routing systems. *Geomorphology*, 316, 1-23.

410 Overeem, I., Nienhuis, J. H., & Piliouras, A. (2022). Ice-dominated Arctic deltas. *Nature*
411 *Reviews Earth & Environment*, 3(4), 225-240.

412 Porritt, E. L., Jones, B. G., Price, D. M., & Carvalho, R. C. (2020). Holocene delta progradation
413 into an epeiric sea in northeastern Australia. *Marine Geology*, 422, 106114.

414 Rhodes, E.G., 1982. Depositional model for a chenier plain, Gulf of Carpentaria, Australia.
415 *Sedimentology*, 29(2), pp.201-221.

416 Rodriguez, A. B., Fassell, M. L., & Anderson, J. B. (2001). Variations in shoreface progradation
417 and ravinement along the Texas coast, Gulf of Mexico. *Sedimentology*, 48(4), 837-853.

418 Ruggiero, P., Kaminsky, G. M., Gelfenbaum, G., & Cohn, N. (2016). Morphodynamics of
419 prograding beaches: A synthesis of seasonal-to century-scale observations of the Columbia
420 River littoral cell. *Marine Geology*, 376, 51-68.

421 Rustomji, P., Shellberg, J., Brooks, A., Spencer, J., & Caitcheon, G. (2010). A catchment
422 sediment and nutrient budget for the Mitchell River, Queensland. *Tropical Rivers and Coastal*
423 *Knowledge (TRACK)*, 1-119.

- 424 Semeniuk, V. (1995). The Holocene record of climatic, eustatic and tectonic events along the
425 coastal zone of Western Australia—a review. *Journal of Coastal Research*, 247-259.
- 426 Sloss, C. R., Nothdurft, L., Hua, Q., O'Connor, S. G., Moss, P. T., Rosendahl, D., ... & Ulm, S.
427 (2018). Holocene sea-level change and coastal landscape evolution in the southern Gulf of
428 Carpentaria, Australia. *The Holocene*, 28(9), 1411-1430.
- 429 Tamura, T. (2012). Beach ridges and prograded beach deposits as palaeoenvironment
430 records. *Earth-Science Reviews*, 114(3-4), 279-297.
- 431 Thampanya, U., Vermaat, J. E., Sinsakul, S., & Panapitukkul, N. (2006). Coastal erosion and
432 mangrove progradation of Southern Thailand. *Estuarine, coastal and shelf science*, 68(1-2),
433 75-85.
- 434 Torgersen, T., Hutchinson, M. F., Searle, D. E., & Nix, H. A. (1983). General bathymetry of the
435 Gulf of Carpentaria and the Quaternary physiography of Lake Carpentaria. *Palaeogeography,*
436 *Palaeoclimatology, Palaeoecology*, 41(3-4), 207-225.
- 437 Weissmann, G. S., Hartley, A. J., Nichols, G. J., Scuderi, L. A., Olson, M., Buehler, H., &
438 Banteah, R. (2010). Fluvial form in modern continental sedimentary basins: distributive fluvial
439 systems. *Geology*, 38(1), 39-42.
- 440 Weissmann, G.S., Hartley, A.J., Scuderi, L.A., Nichols, G.J., Davidson, S.K., Own, A., Atchley,
441 S.C., Bhattacharyya, P., Chakraborty, T., Ghosh, P., Nordt, L.C., Michel, L., & Tabor, N.J.
442 (2013). Prograding distributive fluvial systems—geomorphic models and ancient examples. In
443 Driese, S.G. & Nordt, L.C. (Eds), *New Frontiers in Paleopedology and Terrestrial*
444 *Paleoclimatology: Paleosols and Soil Surface Analog Systems*, SEPM Society for Sedimentary
445 *Geology*, Tulsa, OK, USA, 131-147.
- 446 Wheeler, H.E. (1958). Time Stratigraphy. *AAPG Bulletin*, 42, 1047-1063.
- 447 Wheeler, H.E. (1964). Baselevel, Lithosphere Surface, and Time-Stratigraphy. *Geological*
448 *Society of America Bulletin*, 75(7), 599-610
- 449 Wu, W., & Leonard, M. (2019). Impact of ENSO on dependence between extreme rainfall and
450 storm surge. *Environmental Research Letters*, 14(12), 124043.
- 451 Wu, X., Fernandez, R., Baas, J. H., Malarkey, J., & Parsons, D. R. (2022). Discontinuity in
452 Equilibrium Wave-Current Ripple Size and Shape and Deep Cleaning Associated With
453 Cohesive Sand-Clay Beds. *Journal of Geophysical Research: Earth Surface*, 127(9),
454 e2022JF006771.
- 455 Zuchuat, V., Midtkandal, I., Poyatos-Moré, M., Da Costa, S., Brooks, H. L., Halvorsen, K., ... &
456 Braathen, A. (2019). Composite and diachronous stratigraphic surfaces in low-gradient,
457 transitional settings: The J-3 “unconformity” and the Curtis Formation, east-central Utah, USA.
458 *Journal of Sedimentary research*, 89(11), 1075-1095.